

# Smoothing of Headland Path Edges and Headland-to-Mainfield Lane Transitions Based on a Spatial Domain Transformation and Linear Programming

Mogens Plessen\*

## Abstract

Within the context of in-field path planning and under the assumption of nonholonomic vehicle models this paper addresses two tasks: smoothing of headland path edges and smoothing of headland-to-mainfield lane transitions. Both tasks are solved by a two-step hierarchical algorithm. The first step differs for the two tasks generating either a piecewise-affine or a Dubins reference path. The second step leverages a transformation of vehicle dynamics from the time domain into the spatial domain and linear programming. Benefits such as a hyperparameter-free objective function and spatial constraints useful for area coverage gaps avoidance and precision path planning are discussed. The method, which is a deterministic optimisation-based method, is evaluated on 5 real-world fields solving 19 instances of the first task and 84 instances of the second task.

**Keywords:** In-field path planning; Nonholonomic vehicle dynamics; Linear Programming; Spatial Transformation.

## MAIN NOMENCLATURE

MAIN NOMENCLATURE	
Symbols	
$D_s$	Spatial discretisation spacing, (m).
$R_{\text{Dubins}}$	Radius of Dubins path, (m).
$e_\psi$	Path-aligned relative heading, (deg).
$l$	Wheelbase of vehicle, (m).
$\bar{n}_{\text{cstrts}}$	Average number of inequality constraints, (-).
$\bar{n}_u$	Average number of decision variables, (-).
$(s, e_y)$	Path-aligned position coordinates, (m).
$v$	Velocity, (m/s).
$w$	Operating width (inter-lane distance), (m).
$(x, y)$	Global position coordinates, (m).
$\delta$	Steering angle of vehicle, (deg).
$\psi$	Global absolute heading, (deg).
$\rho_s$	Radius of curvature, (m).
$\bar{\tau}$	Average solution runtime, (s).
Abbreviations	
LP	Linear Programming.
PWA	Piecewise-Affine.
UTM	Universal Transverse Mercator coordinate system.

## 1. Introduction

Logistics play a large role in agriculture. For arable farming and the cultivation of crops it can be differentiated between in-field and inter-field logistics (Plessen (2019a)). For the former, efficient path planning is of interest subject to three main considerations: (i) minimisation of tractor traces within the field in order to maximize growable field area, (ii) minimisation of area coverage pathlength in order to minimize fuel consumption and time spent in the field, and (iii) avoiding area coverage

gaps such that the entire field is covered, for example during a field-run spraying herbicide or pesticide applications, while simultaneously accounting for a given operating width of the machinery operating in the field and accounting for its typically nonholonomic vehicle dynamics, state and actuator constraints.

Within this context the motivation and contribution of this paper is to present a method for smoothing of headland path edges and headland-to-mainfield lane transitions based on a spatial domain transformation and linear programming. As will be motivated below, the spatial domain transformation permits to formulate spatial constraints useful for precision path planning in agriculture. A linear programming framework with a hyperparameter-free objective function can incorporate those constraints together with linearised and discretised nonholonomic vehicle dynamics in a disciplined manner to produce deterministic precision paths and fast solve times.

This research topic is of interest to both autonomous robot applications as well as for manual driving by providing a guidance reference to a human driver. Relevance is underlined, first, by the ubiquity of headland path and headland-to-mainfield lane transitions for every field coverage, and, second, by the nonlinear nature of the problem for nonholonomic vehicle dynamics.

Thus, given an optimised sequence of mainfield lane traversals for field coverage such as produced in Plessen (2019b) and Plessen (2018), this paper provides a method for path smoothing. See also Höffmann et al. (2024), Mier et al. (2023), Khan et al. (2016) for more high-level area coverage techniques. This paper differs from Plessen & Bemporad (2017), where an *on-line* closed-loop tracking controller based on model predictive control was presented, in that here the focus is on *offline* generation of precision paths, which might then afterwards be tracked online by the approach from aforementioned paper or an alternative closed-loop tracking controller.

A widespread approach to reference path and in particular

\*MP is with Findklein GmbH, Switzerland, mgplessen@gmail.com

headland turn trajectory generation is to build methods around specific path planning *patterns*. A literature review is provided. In Trendafilov & Tihanov (2022) 5 types of T-turns are considered. In Wang & Noguchi (2018) adaptive turning based on a switchback-pattern and dynamic circleback-pattern is discussed. In Sabelhaus et al. (2013) 9 different symmetric lane-to-lane transitions are analysed, including Omega-turn, U-turn, gap-turn and fishtail-turn. Similarly, Backman et al. (2015) account for maximum steering rate and the maximum acceleration of the vehicle. In Bulgakov et al. (2019) for a trailed asymmetric swath reaper–tractor aggregate a pear-shaped loop-turn and a U-turn are discussed. In Boryga et al. (2020) 4 types of patterns are discussed, whereby each is composed of two transition curves. In Peng et al. (2023) an optimisation-based method for turning in constrained headland spaces such as orchards is presented, using 4 types of turns (U-turn, Omega-turn, switchback-turn and circleback-turn) for generation of a first reference path. Gao et al. (2023) use Bezier curves for a headland-turning navigation system for a safflower picking robot. Finally, see Ha et al. (2018) for an example of a hardware modification to facilitate headland turning.

Once a smooth path plan is computed, for autonomous robots a plethora of techniques for online tracking can be applied, see e.g. Wang et al. (2023), Etefagh et al. (2018), He et al. (2023), Wang et al. (2024), Sun et al. (2024), Liu et al. (2024), Eski & Kuş (2019), Jing et al. (2021), Yin et al. (2020). For a recent overview of control algorithms of autonomous all-terrain vehicles in agriculture see Etezadi & Eshkabilov (2024).

The research gap and motivation for this paper is discussed. First, the focus of aforementioned pattern-based references is on lane-to-lane transitions. Second, an issue for pattern-based path planning, in particular based on straights, arcs and clothoid segments, is that resulting paths are typically operating at actuation limits such as maximum curvature and maximum steering rate. For general headland path smoothing (in contrast to aforementioned lane-to-lane transitions) this is not sufficient where other constraints such as area coverage gaps must also be accounted for. Third, the proposal of a spatial domain transformation in order to be able to formulate optimisation problems with spatial constraints, which is desirable for precision agriculture applications, is missing in the literature.

The focus of this paper is on path planning instead of path tracking. The allure of a numerical optimisation approach is that it allows incorporation of a variety of constraints in a disciplined manner and can handle the multivariate nature of the task. The allure of transforming vehicle dynamics from the time into the spatial domain is that it allows to formulate spatial precision constraints. An early paper discussing benefits of transformations of dynamics from the time into the spatial domain is Pfeiffer & Johanni (1987). To the author’s knowledge this is the first paper that proposes a spatial transformation of system dynamics to calculate precision path plans in agriculture.

The remaining paper is organised as follows: problem formulation, modeling and proposed solution, numerical results and the conclusion are described in Sections 2-6.

## 2. Problem Formulation

Figure 1 introduces basic terminology. In a first step, with the objective of generating an area covering path for a given field in mind, a lane-grid consisting of a headland path and mainfield lanes is generated, see Fig. 2. Therefore, the field contour is eroded to generate the headland path, before mainfield lanes are fitted. Mainfield lanes can either be straight lanes or freeform lanes, for example, adapted in shape using a partial segment of the headland path as reference. See Plessen (2021) for the generation of freeform lanes and a comparison to straight lanes for the minimisation of the total number of mainfield lanes. The inter-lane distance is selected as the machinery operating width denoted by  $w > 0$ .

After generating a lane-grid and under the assumption that the field shall be covered by a nonholonomic vehicle, two problem types arise. Both evolve around the smoothing of edges to generate a path suitable for nonholonomic vehicle dynamics, either along the headland path or at the transitions between mainfield lanes and the headland path.

**Problem 1.** *Given a headland path determine edgy path segments along it and correct them such that a smoothed headland path is generated that is (i) suitable for nonholonomic vehicle dynamics and (ii) avoiding area coverage gaps.*

**Problem 2.** *Given headland-to-mainfield lane transitions, and vice versa mainfield lane-to-headland transitions, as part of a field covering path, correct those if necessary such that smoothed transitions are generated that are (i) suitable for nonholonomic vehicle dynamics and (ii) avoiding area coverage gaps.*

The proposal of an algorithm for the solution of Problems 1 and 2 is the topic of this paper.

## 3. Proposed Solution

The general approach to address both Problems 1 and 2 is a hierarchical two-step algorithm. The first step differs for the two problems and has as objective the generation of a reference path. The second step uses that reference path and leverages linear programming and a transformation of vehicle dynamics from the time into the spatial domain.

### 3.1. Spatial Domain Transformation

To illustrate the spatial domain transformation and for simplicity, the method is illustrated for a kinematic bicycle model. It is referred to Plessen et al. (2017a) for handling of more complex vehicle models.

This section summarizes the notation of Plessen et al. (2017b). Consider a *global* and a *path-aligned* coordinate frame within the  $(x, y)$ - and  $(s, e_y)$ -plane, respectively, with path centerline coordinate  $s \geq 0$  and lateral deviation  $e_y \in \mathbb{R}$ . Coordinates can be transformed by projecting point masses (vehicle’s center of gravity) to piecewise-affine path segments. As a detail, it can be differentiated between the path centerline coordinate  $s \geq 0$ , and actual path length coordinate  $\eta \geq 0$ , indicating

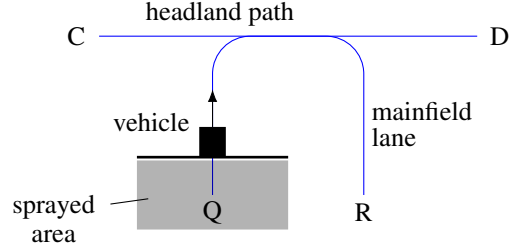
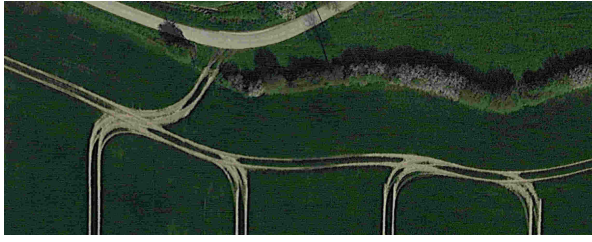


Fig. 1. *Left*: Visualisation of real-world transitions between headland path and mainfield lanes. As illustrated, the transitions between headland path and mainfield lanes can be “messy” in the sense that these often cause an increased amount of compacted field areas due to crossings of tyre traces. *Right*: Abstract visualisation with the definitions of headland path and mainfield lanes along which a vehicle (e.g., with spraying implement) might travel from location Q towards R or D.

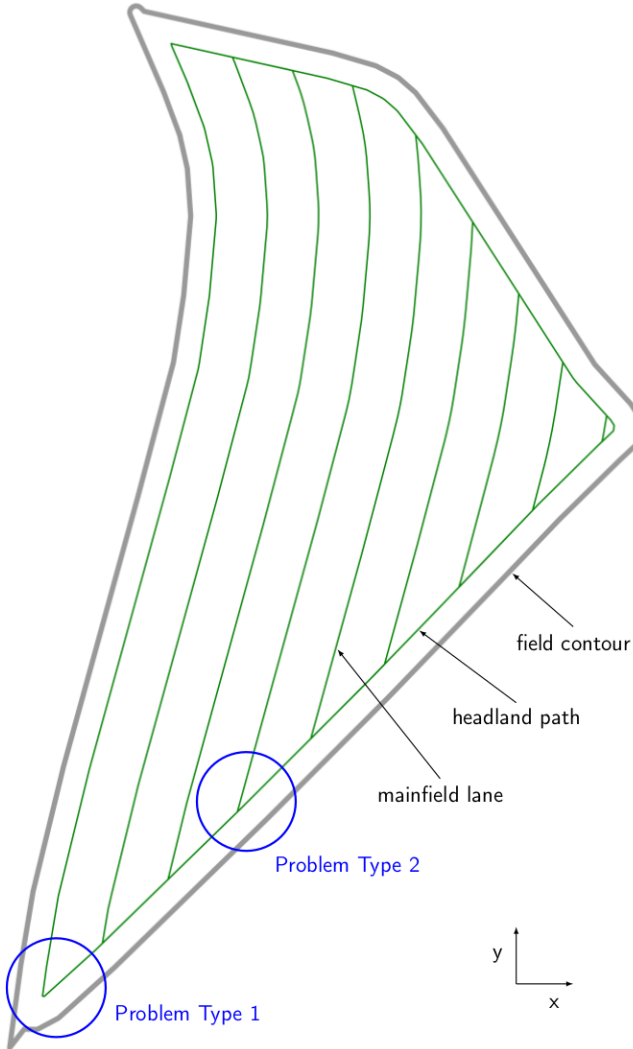


Fig. 2. Illustration of terminology and visualisation of Problem 1 and 2.

the distance traveled by the vehicle. Note that  $\eta \neq s$ , unless the vehicle is traveling perfectly along the path centerline. A trajectory can then be defined as  $z(s) = [e_\psi(s), e_y(s)]$ , with heading deviation  $e_\psi(s) \in [0, 2\pi]$  at coordinate  $s$ . The equivalent trajectory in the  $(x, y)$ -plane is defined by  $X(s) = [x(s), y(s), \psi(s)]$ . The classic nonlinear kinematic bicycle model Rajamani (2011) is

$$\begin{bmatrix} \dot{x} \\ \dot{y} \\ \dot{\psi} \end{bmatrix} = \begin{bmatrix} v \cos(\psi) \\ v \sin(\psi) \\ \frac{v}{l} \tan(\delta) \end{bmatrix}, \quad (1)$$

assuming the center of gravity to be located at the rear axle and  $l$  denoting the wheelbase. The front-axle steering angle is  $\delta$  and vehicle velocity is  $v$ . Let us denote time and spatial derivatives by  $\dot{x} = \frac{dx}{dt}$  and  $x' = \frac{dx}{ds}$ , respectively. The spatial equivalent of (1) is derived as follows. By  $\dot{e}_\psi = \dot{\psi} - \dot{\psi}_s$  where  $\psi_s \in [0, 2\pi]$  the path heading,  $\dot{e}_y = v \sin(e_\psi)$ ,  $\dot{s} = \frac{\rho_s v \cos(e_\psi)}{\rho_s - e_y}$  where  $\rho_s$  denotes the radius of curvature,  $e'_\psi = \frac{\dot{e}_\psi}{\dot{s}}$  and  $e'_y = \frac{\dot{e}_y}{\dot{s}}$ , we obtain

$$\begin{bmatrix} e'_\psi \\ e'_y \end{bmatrix} = \begin{bmatrix} \frac{(\rho_s - e_y) \tan(\delta)}{\rho_s l \cos(e_\psi)} - \psi'_s \\ \frac{\rho_s - e_y}{\rho_s} \tan(e_\psi) \end{bmatrix}. \quad (2)$$

Importantly, (2) is entirely independent of vehicle speed  $v$ . This is characteristic for kinematic models, but not the case for dynamic vehicle models (Plessen et al. (2017a)). Furthermore, note that (2) has one state dimension less than (1). To summarize, we define spatially-dependent state and control vectors as  $z = [e_\psi, e_y]$  and  $u = [\delta]$ , respectively. We abbreviate (2) by  $z' = f(z, u)$ . Let a discretisation grid along the path centerline be defined by  $\{s_j\}_{j=0}^N = \{s_0, s_1, \dots, s_N\}$ . For the remainder of this paper, index  $j$  refers to the spatial discretisation grid. The discretisation grid can be uniformly spaced. Additional grid points can be added. For a given set of references  $\{e_{\psi,j}^{\text{ref}}\}_{j=0}^N$ ,  $\{e_{y,j}^{\text{ref}}\}_{j=0}^N$  and  $\{u_j^{\text{ref}}\}_{j=0}^{N-1}$  and initial state, the linearised and discretised (zero-order hold) state dynamics of (2) can be computed for  $\{e_{\psi,j}\}_{j=0}^N$  and  $\{e_{y,j}\}_{j=0}^N$  as a function of control inputs  $\{\delta_j\}_{j=0}^{N-1}$ . Continuous rate constraints on steering are,

$$\delta_{\min} \leq \dot{\delta} \leq \delta_{\max}, \quad (3)$$

whereby the bounds,  $\delta_{\min}$  and  $\delta_{\max}$ , in general, are nonlinear functions of the vehicle’s operating point and time-varying parameters. By applying the spatial coordinate transformation, a discretisation, a change of variables, and assuming the bounds to remain constant over the planning horizon, we obtain

$$\frac{D_{s,j} \dot{\delta}_{\min}(\rho_{s,j} - e_{y,j})}{\rho_{s,j} \cos(e_{\psi,j}) v_j} \leq \delta_{j+1} - \delta_j \leq \frac{D_{s,j} \dot{\delta}_{\max}(\rho_{s,j} - e_{y,j})}{\rho_{s,j} \cos(e_{\psi,j}) v_j}, \quad (4)$$

whereby we abbreviated  $D_{s,j} = s_{j+1} - s_j$ . Thus, linear rate constraints in (3) are rendered not only nonlinear, but also state-dependent and also velocity-dependent. This has two implications. First, to formulate linearly constrained optimisation problems, in general, we require the linearisation of (4). Dependent on the quality of underlying reference trajectories, this may incur significant distortions. Second, while the discrete form of (3) can always be guaranteed to be feasible (assuming a feasible initialisation), for (4) this is not the case anymore. Let us consider two degrees of simplification of (4). First, we assume small  $e_{\psi,j}$  and  $e_{y,j}$ , and consequently approximate  $\frac{(\rho_{s,j} - e_{y,j})}{\rho_{s,j} \cos(e_{\psi,j})} \approx 1$ , thereby rendering (4) state-independent, but maintaining velocity-dependent bounds. Thus, steering rate constraints still depend on  $v_j$ . Second, we additionally eliminate this velocity-dependency and formulate

$$\frac{D_{s,j}}{v_{\text{ref}}} \delta_{\text{min}} \leq \delta_{j+1} - \delta_j \leq \frac{D_{s,j}}{v_{\text{ref}}} \delta_{\text{max}}, \quad j = 0, \dots, N-2, \quad (5)$$

whereby,  $v_{\text{ref}} > 0$  is introduced as a reference velocity parameter choice. Formulation (5) bears the advantage of eliminating state dependency and is therefore our preferred form for spatial rate constraints. In practice, we employ bounds that are constant over the spatial planning horizon, but in general time-varying in any closed-loop receding horizon control-setting and dependent on the vehicle's operating point.

To summarize this section, the transformation of time-dependent control rate constraints (3) to the path-aligned coordinate frame is not trivial and to be considered as the main disadvantage of a spatial-based system representation. We opted for the simple state-independent form (5) for linearly constrained optimisation problems, and discussed the role of  $v_{\text{ref}} > 0$  as a transformation parameter.

Finally, we draw an important analogy to clothoid and continuous curvature path planning methods to further justify above approach for the handling of rate constraints in the spatial domain. Continuous curvature and clothoid based path planning methods such as in Sabelhaus et al. (2013) typically assume bounds on 'curvature' and 'sharpness' (the change in curvature) resulting in piecewise-affine curvature profiles along the planned path. Note that this implicitly also assumes an approximation of steering rate constraints.

### 3.2. Main Two-Step Hierarchical Algorithm

The following high-level algorithm is proposed to address both Problem 1 and 2:

Pre-processing: Determine an edgy path segment.

1. Fit an approximating path that shall serve as reference in the subsequent step.
2. Solve a linear program (LP) based on spatial transformation of nonholonomic vehicle dynamics and the reference path from Step 1 to generate a smoothed path.

Post-processing: Replace the edgy path segment with the smoothed path.

An edgy path segment can either be a headland path segment or a headland-to-mainfield lane transition. Edgy path segments are identified by heuristics, in particular, by searching for abrupt heading-changes above a certain threshold as well as the labeling of path coordinates as headland path or mainfield lane and detecting their changes.

**Remark 1.** *The focus here is on linear programming. In general, also any other objective function can be possible, for example, a quadratic program. However, as shown below a linear programming is sufficient and permits to formulate a hyperparameter-free objective function.*

The next two subsections discuss differences of Step 1 and Step 2 for the two Problems 1 and 2.

### 3.3. Problem 1: Headland path smoothing

The two steps of the hierarchical algorithm for Problem 1 are visualised in Fig. 3. The illustrative edgy headland path segment is the one labeled with *Problem Type 1* in Fig. 2. First, this segment is scaled by heuristics and replaced by a 5-point piecewise-affine (PWA) path as shown in Fig. 3(a). Underlying notion for this scaling is that the tip of the resulting 5-point PWA path ensures zero spraying gap. Thus, the distance between tip and its projection point along the field contour must be less or equal than half the machinery operating width  $w > 0$ .

As a detail, we do not use popular Chaikin's algorithm (see Chaikin (1974)) for corner cutting, since this would replace every edge point with two edge points at each iteration step. Furthermore, it would cut off a significant portion of the tip of the 5-point PWA line after the first iteration.

Using the 5-point PWA path from Step 1 as reference path for Step 2 of the hierarchical algorithm and Problem 1 the following basic LP is proposed:

$$\min_{\{\delta_j\}_{j=0}^{N-1}} \sum_{j=1}^N |e_{y,j} - e_{y,j}^{\text{ref}}| \quad (6a)$$

$$\text{s.t. } e_{y,j} - e_{y,j}^{\text{ref}} \leq 0, \quad j = 1, \dots, N, \quad (6b)$$

$$D_{s,j} \frac{\delta_{\text{min}}}{v_{\text{ref}}} \leq \delta_{j+1} - \delta_j \leq D_{s,j} \frac{\delta_{\text{max}}}{v_{\text{ref}}}, \quad j = 0, \dots, N-2, \quad (6c)$$

$$\delta_{\text{min}} \leq \delta_j \leq \delta_{\text{max}}, \quad j = 0, \dots, N-1, \quad (6d)$$

with  $D_{s,j} = s_{j+1} - s_j, \forall j = 0, \dots, N-2$ .

In practice, constraints (6b) which enforce the resulting path to stay on one side of the reference path are relaxed to,  $e_{y,j} - e_{y,j}^{\text{ref}} \leq \sigma$ , by introducing a non-negative slack variable  $\sigma \geq 0$  and adding it to the objective function 6a with a high weight such that  $\sum_{j=1}^N |e_{y,j} - e_{y,j}^{\text{ref}}|$  is replaced with  $\sum_{j=1}^N |e_{y,j} - e_{y,j}^{\text{ref}}| + 10^{16} \sigma$ . Furthermore, for the absolute value arguments  $N$  non-negative surrogate variables are introduced and the set of inequality constraints is extended accordingly. In the end, there are  $n_u = 2N + 1$  scalar real-valued optimisation variables. Typical sizes of the LP (i.e., the number of variables and inequality constraints) are stated in the numerical example Section 4.

For generality, reference  $e_{y,j}^{\text{ref}}$  is included in (6). In practice, it is typically set to zero,  $e_{y,j}^{\text{ref}} = 0, \forall j = 1, \dots, N$ .

One benefit of proposed formulation (6) is that it is hyperparameter-free. There are no weighting parameters.

An even smaller alternative LP was considered, with a minmax-objective function,  $\min_{\{\delta_j\}_{j=0}^{N-1}} \max_{j \in \{1, \dots, N\}} |e_{y,j} - e_{y,j}^{\text{ref}}|$ , replacing (6a). However, this was found to be unsuited since only the maximum deviation from the reference path would be penalised, which resulted in jagged trajectories not accurately tracking the complete reference path.

After the solution of (6), a smoothed headland path segment as shown in Fig. 3(b) results.

Finally, *LP-iterations* or refinement steps can be conducted. Thus, for the first solution of (6) a 5-point-PWA path is used as reference. Then, the resulting path is used as reference for the second solution of (6). In theory, many of such LP-iterations can be carried out. In practice, one refinement step was found to be useful and sufficient.

### 3.4. Problem 2: Headland-to-mainfield lanes transitions

Before stating the LP for Problem 2, the term *headland-to-mainfield lanes* transitions is clarified. It is used comprehensively for brevity but shall always refer to both, (i) transitions from headland to a mainfield lane, but also (ii) transitions from a mainfield lane to the headland path. Both types of transitions naturally occur for a field coverage path. As will be shown below, a subtle difference in constraints formulation is applied to differentiate the two types.

The following basic LP is proposed for Problem 2:

$$\min_{\{\delta_j\}_{j=0}^{N-1}} \sum_{j=1}^N |e_{y,j} - e_{y,j}^{\text{ref}}| \quad (7a)$$

$$\text{s.t. } D_{s,j} \frac{\delta_{\min}}{v_{\text{ref}}} \leq \delta_{j+1} - \delta_j \leq D_{s,j} \frac{\delta_{\max}}{v_{\text{ref}}}, \quad j = 0, \dots, N-2, \quad (7b)$$

$$\delta_{\min} \leq \delta_j \leq \delta_{\max}, \quad j = 0, \dots, N-1, \quad (7c)$$

with  $D_{s,j} = s_{j+1} - s_j, \forall j = 0, \dots, N-2$ .

In practice, the objective function (7a) is slightly refined to better avoid undesired overshoots out of the mainfield area and into the headland area. Therefore, (7a) is replaced with  $\sum_{j=1}^N c_j |e_{y,j} - e_{y,j}^{\text{ref}}|$  and weights

$$c_j = \begin{cases} 100 & j = 1, \dots, I \\ 1 & j = I+1, \dots, N \end{cases}$$

for transitions from headland to a mainfield lane, and

$$c_j = \begin{cases} 1 & j = 1, \dots, I-1 \\ 100 & j = I, \dots, N \end{cases}$$

for transitions from mainfield lane to the headland path, where index  $I$  is computed from the reference path as its last and first index within a 1m-radius to the headland path for the two transition types, respectively. The value 100 is selected exemplarily and can be any large constant, such that the objective function of the LP can still be considered hyperparameter-free. The benefit of this weighted approach is that no additional inequality

constraints need to be introduced. As a result, LP (7) for Problem 2 is smaller than LP (6) for Problem 1.

As for above LP (6), for the absolute value arguments in (7a)  $N$  non-negative surrogate variables are introduced and the set of inequality constraints is extended accordingly. In the end, there are  $n_u = 2N$  scalar real-valued optimisation variables. Typical sizes of the LP (i.e., the number of variables and inequality constraints) are stated in the numerical example Section 4. As in the previous subsection, reference  $e_{y,j}^{\text{ref}}$  in (7) is typically set to zero,  $e_{y,j}^{\text{ref}} = 0, \forall j = 1, \dots, N$ .

Fig. 5 visualizes the result of a headland-to-mainfield lane transition. As part of Step 1 of the hierarchical algorithm for Problem 2 a Dubins path is fitted and replacing the edgy original transition. The Dubins path, plus an additional small path segment before and after selected based on heuristics to permit additional maneuvering space, serves as reference to Step 2 of the hierarchical algorithm based on which (7) is formulated and solved.

Fig. 5 is of special interest for two reasons. First, it illustrates how Dubins paths are *not* suited for the generation of precision paths to be followed by autonomous machines online, especially when calculating Dubins paths with minimal turning radius of the machine (see Fig. 5(a)). Due to actuation constraints deviations would be expected in any online tracking application. Second, it illustrates the effect on tracking performance when using different turning radii  $R_{\text{Dubins}}$  in the Dubins reference path generation step. When using the minimal turning radius Fig. 5(a) results. By using an artificially larger  $R_{\text{Dubins}}$  the LP-solution trajectory follows more closely the reference path, see Fig. 5(b) and 5(c). The drawback of a larger  $R_{\text{Dubins}}$  is that the resulting path is longer and more compacted area occurs from corresponding tyre traces and the corresponding steering maneuvers, which reduces growable crop area in the field area. A trade-off with a preference towards small  $R_{\text{Dubins}}$  for the reference path generation step is recommended.

Finally, in contrast to Problem 1 and its discussion in Section 3.3 for the case of Problem 2 no LP-iterations are conducted. It was empirically found that they did not improve results and are therefore omitted.

### 3.5. Discussion of Parameters and Practical Details

This section elaborates on important parameter choices and other practical details.

First, the selection of discretisation spacing,  $D_{s,j} = s_{j+1} - s_j, \forall j = 0, \dots, N-1$ , is discussed, which typically is selected as uniformly spaced but can also be non-uniformly spaced. Its importance for spatial-based numerical optimisation is underlined. Its selection influences on one hand the size of the LPs (the larger the spacing the smaller the LP) and on the other hand the feasibility and quality of resulting trajectories. The smaller the spacing the more danger of generating jaggedness as sketched in Fig. 6, whereas the larger the spacing the more resulting trajectories obtain piecewise-affine and thus edgy shape. The danger of generating jaggedness as sketched in Fig. 6 is an intrinsic and main disadvantage of all spatial-based optimisation problem formulations. On the other hand,

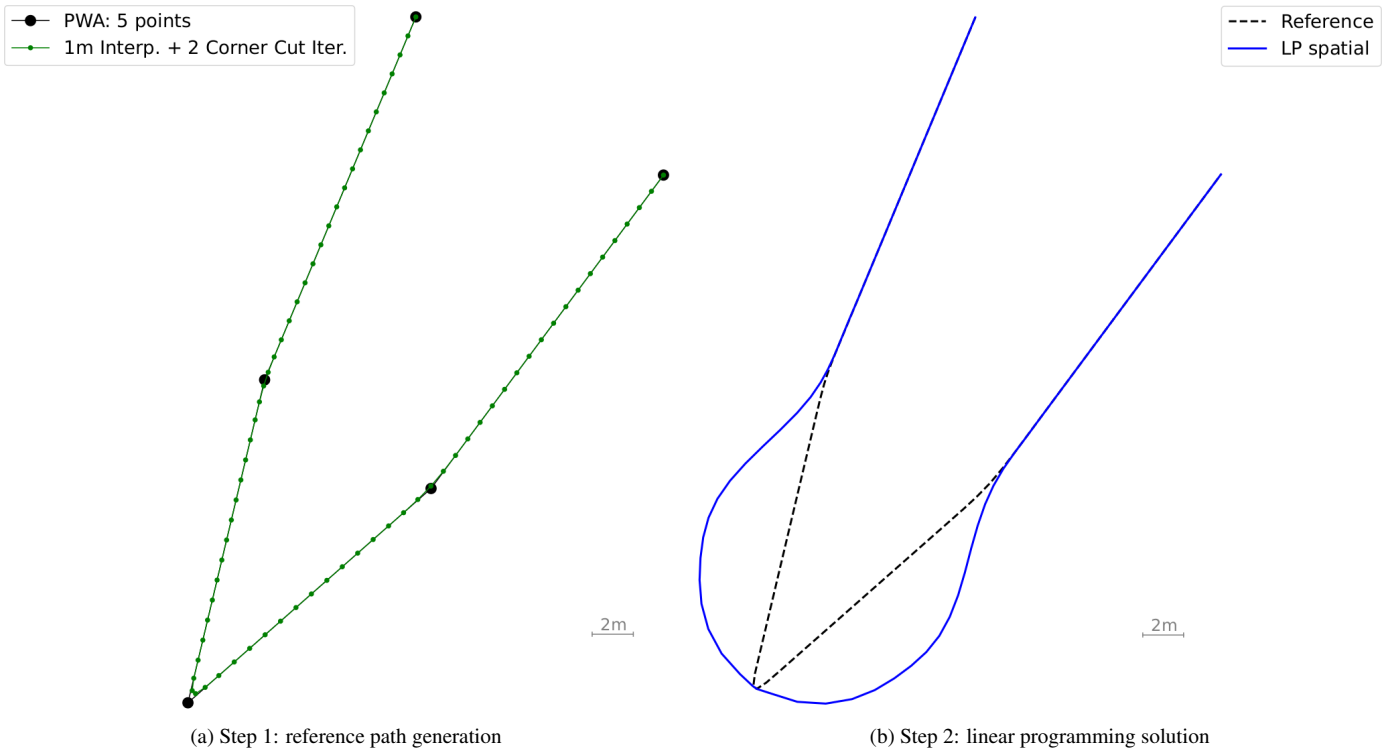


Fig. 3. Problem 1: headland path smoothing. Illustration of two hierarchical steps: (a) generation of a reference (a 5-point piecewise-affine fit that is subsequently interpolated and smoothed via two corner cut-iterations), before (b) using that reference in combination with a spatial domain transformation for a linear program.

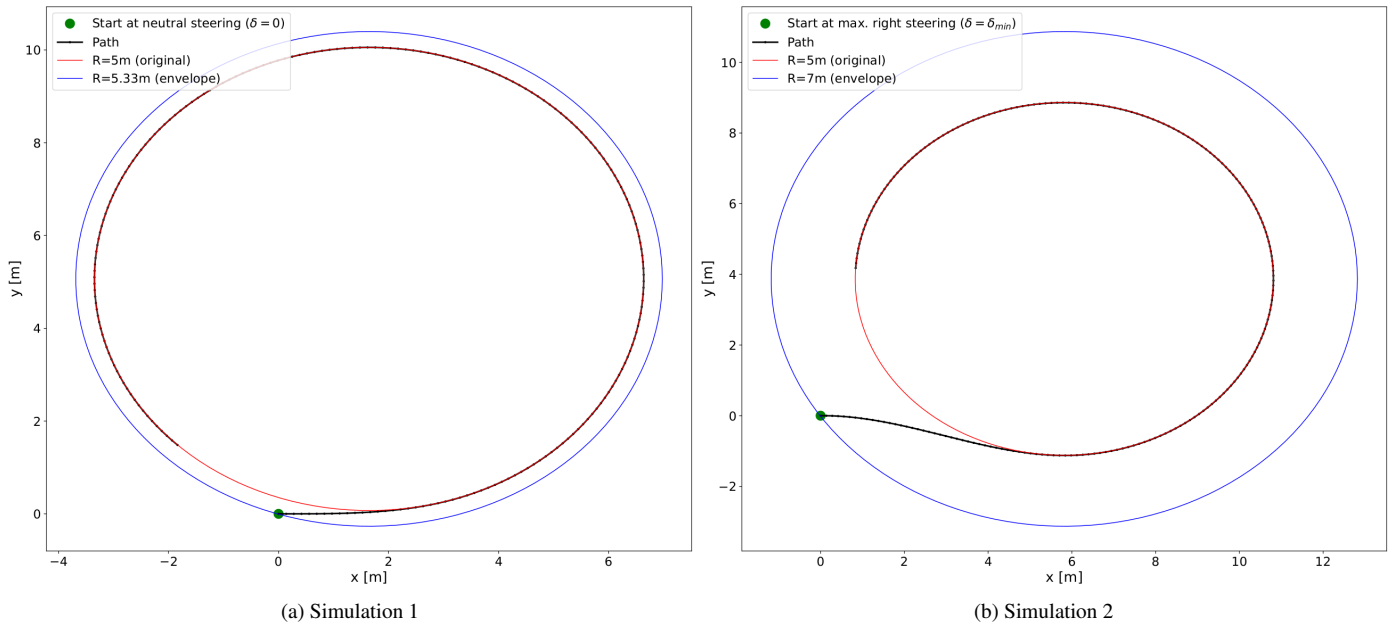


Fig. 4. Given an initial vehicle position  $[x(t), y(t), \psi(t)] = [0, 0, 0]$  and either  $\delta(t) = 0$  or  $\delta(t) = \delta_{\min}$  as initial steering at time  $t = 0$ , two simulations are conducted, applying maximum possible steering at each sampling time according to the law,  $\delta(t + T_s) = \max\{\delta(t) + T_s \dot{\delta}_{\max}, \delta_{\max}\}$  for all  $t > 0$ . The effect of steering rate constraints on the transition phase, before the vehicle reaches its minimum turning radius, is visualised. Enveloping circles are fitted. The effect of using different radii of the envelope circles for reference path generation is visualised in Fig. 5.

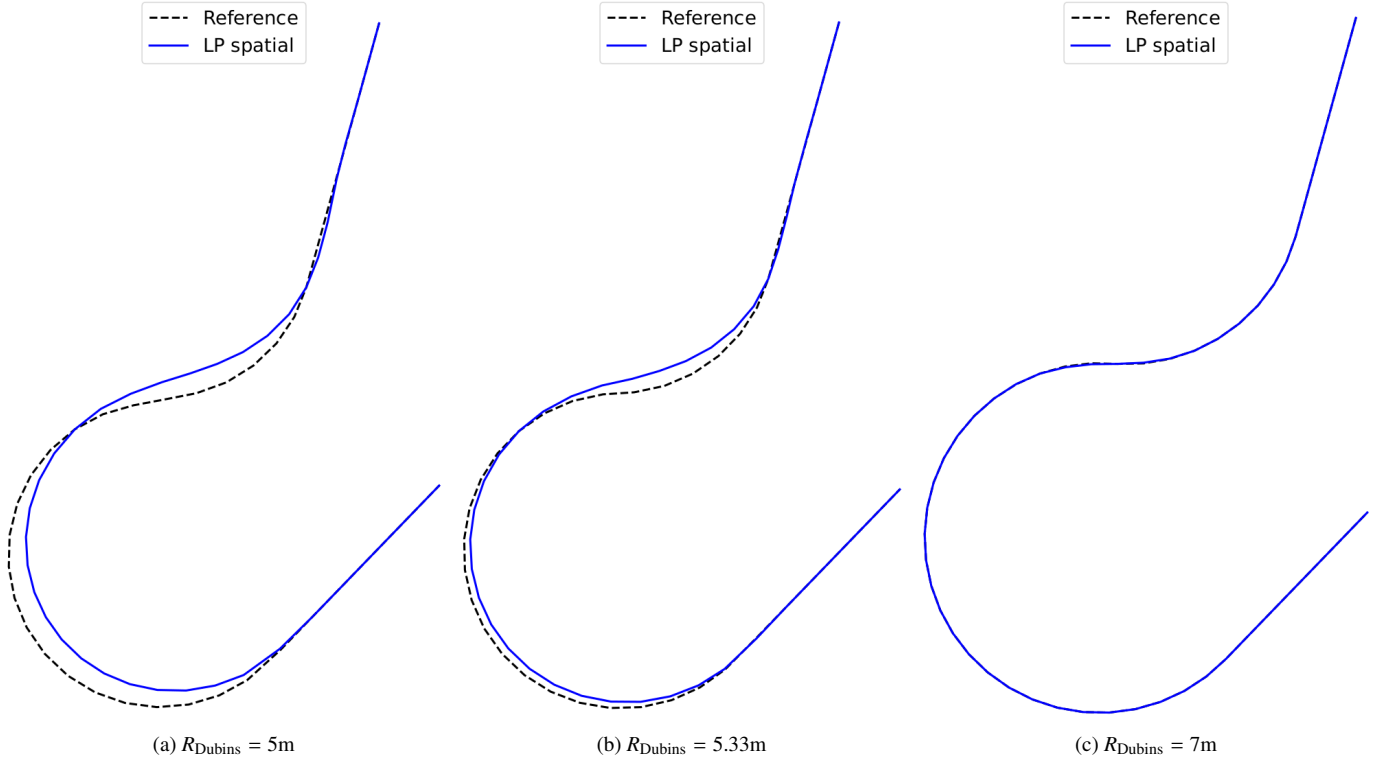


Fig. 5. Problem 2: The effect on tracking performance when using three different  $R_{\text{Dubins}}$  in the reference path generation step is visualised. The drawback of a larger  $R_{\text{Dubins}}$  is that the resulting path is longer and more compacted field area occurs from corresponding tyre traces and steering maneuvers, which reduces growable crop area. A trade-off with tendency towards small  $R_{\text{Dubins}}$  is recommended.

in the case of typical uniform spacing for a constant  $D_s > 0$  and  $D_{s,j} = D_s, \forall j = 0, \dots, N - 1$ , there is only a single hyperparameter that can be well tuned. In practice, this can be done either by trial-and-error for a given field or by a worst-case simulation analysis for given system dynamics and actuation limits. In case of in-field path planning, where there typically are no fast-moving obstacle avoidance requirements and precision path trajectories are calculated offline, worst-case simulation analysis reduces to looping over complex Dubins reference paths, calculating spatial-based LP-tracking solutions and evaluating feasibility and tracking error for a given discretisation spacing candidate  $D_s > 0$ . For the numerical experiments in the next section  $D_s = 1\text{m}$  is set for all instances of both Problem 1 and 2.

Second, for Problem 1 a comment about the generation of a reference path is made. The presented 5-point PWA heuristic with tip-scaling serves the objective of spraying gap avoidance. However, it may not be optimal with respect to pathlength minimisation. For example, a simpler 3-point PWA heuristic might also be used as reference path. Heuristic variations on the reference path generation step taking local field contour shape information into account are the subject of future research.

#### 4. Results

For numerical evaluation the field from Fig. 1 is considered. It has a size of 4.5ha and requires the solution of 3 instances of Problem 1 and 16 instances of Problem 2. The field under

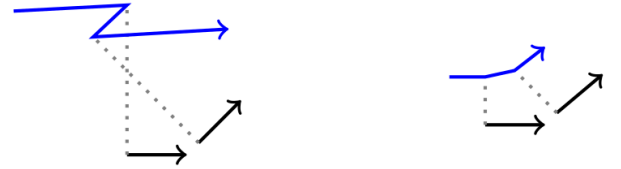


Fig. 6. Sketch illustrating the danger of jaggedness for spatial-based optimisation, where characteristically along a space coordinate a lateral offset  $e_y(s)$  (or  $e_{y,j} = e_y(s_j)$  in the discretised case) is assigned. The two key tuning knobs to avoid jaggedness are (i) selection of a suitable reference path such that resulting lateral deviations are close to the reference path, and (ii) selection of a suitable discretisation spacing  $D_{s,j} = s_{j+1} - s_j, \forall j = 0, \dots, N - 1$ .

Parameter	$l$	$\delta_{\max}$	$\dot{\delta}_{\max}$	$v_{\text{ref}}$
Value	3m	31deg	15deg/s	5km/h

Table 1. Parameters used throughout all numerical experiments. The value  $\delta_{\max} = 31\text{deg}$  was set such that for a minimum turning radius of  $R_{\text{Dubins}} = 5\text{m}$ , it holds  $R_{\text{Dubins}} = \frac{l}{\tan(\delta_{\max})}$ .

$\bar{n}_{\text{cstrts}}$	$\bar{n}_{\text{u}}$	$\bar{\tau}_{\text{LP}}$	$\bar{\tau}_{\text{Bezier}}$
294	149	0.008s	0.002s

Table 2. Average number of constraints  $\bar{n}_{\text{cstrts}}$  and average number of variables  $\bar{n}_{\text{u}}$  of the LPs, and corresponding average solution runtimes for the LP- and Bezier-approach for 3 instances of Problem 1 in Figure 7.

[0, 16, 15, 14, 13, 12, 11, 10, 9, 17, 8, 7, 6, 5, 4, 3, 2, 1, 0, 16, 15, 2, 3, 14, 13, 4, 5, 12, 11, 6, 7, 10, 9, 8, 7, 6, 5, 4, 3, 2, 1, 16, 0], operating width 20m

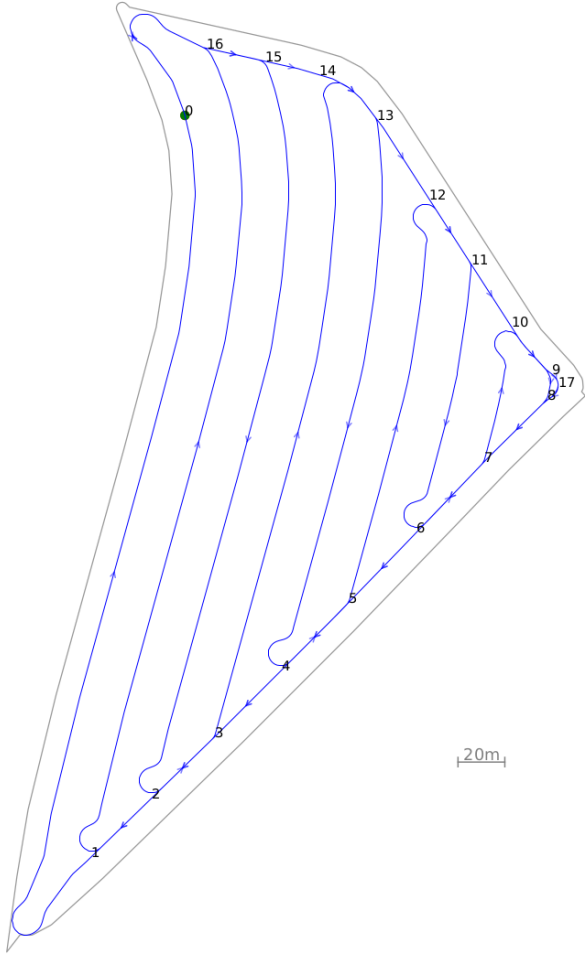


Fig. 7. Experiment: 3 instances of Problem 1 and 16 instances of Problem 2 needed to be solved. The path obtained from proposed method is visualised. The sequence of nodes, [0, 16, ...], gives rise to a full field coverage path plan with node 0 denoting the field entrance. The inter-lane distance is 20m.

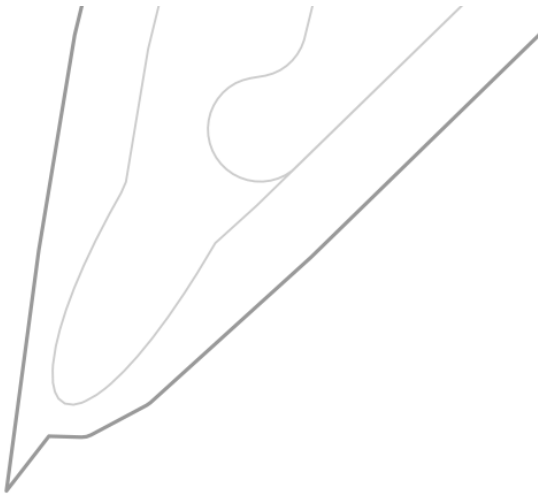


Fig. 8. Illustration of a Bezier curve-fit of third order.

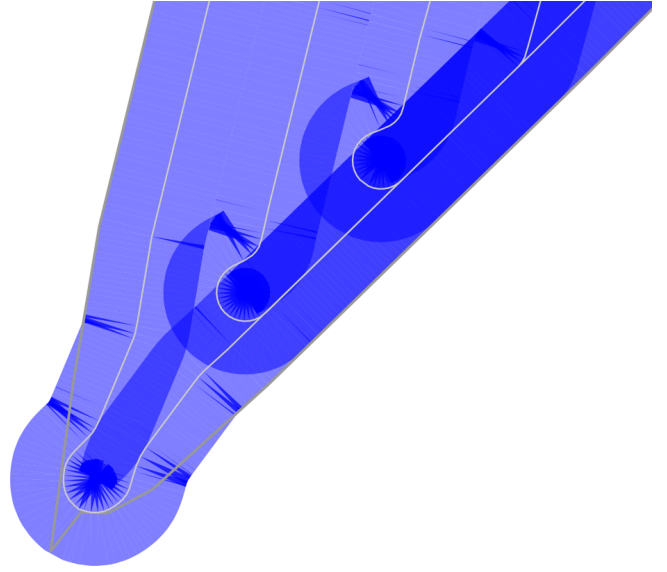


Fig. 9. Zoom-in displaying sprayed coverage area (blue) for the path plan of Fig. 7. Darker blue areas imply overlapping spray area. In this illustrating simulation no section control with individual switching of spray nozzles is assumed (which could in practice reduce the overlapping area).

$\bar{n}_{\text{cstrts}}$	$\bar{n}_u$	$\bar{\tau}_{\text{LP}}$	$\bar{\tau}_{\text{Dubins}}$
98	50	0.0017s	0.0004s

Table 3. Average number of constraints  $\bar{n}_{\text{cstrts}}$  and average number of variables  $\bar{n}_u$  of the LPs, and corresponding average solution runtimes for the LP- and Dubins-solution for 16 instances of Problem 2 in Figure 7.

$R_{\text{Dubins}}$	$\text{mean}\{e_{y,\text{abs}}^{\text{max}}\}$	$\text{max}\{e_{y,\text{abs}}^{\text{max}}\}$
5m	0.32m	0.97m
5.33m	0.16m	0.48m
7m	0.01m	0.04m

Table 4. Average maximum absolute deviation from a Dubins reference path,  $\text{mean}\{e_{y,\text{abs}}^{\text{max}}\}$ , and maximum maximum absolute deviation,  $\text{max}\{e_{y,\text{abs}}^{\text{max}}\}$ , over 16 instances of Problem 2 for three different  $R_{\text{Dubins}} \in \{5\text{m}, 5.33\text{m}, 7\text{m}\}$ . See Fig. 5 for visualisation of one of such instances.



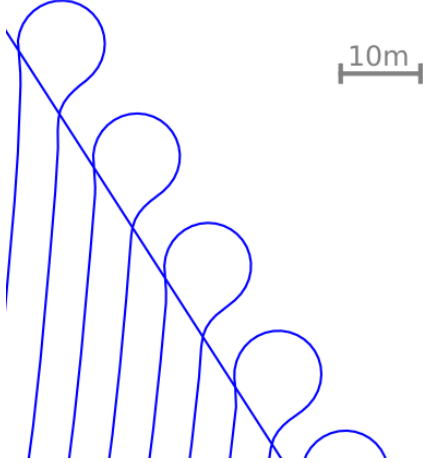


Fig. 10. Extending discussion. Proposed method can also be used for direct transitions between pairs of mainfield lanes. In this illustration, for non-symmetric mainfield lane start and end positions, pear-shaped steering maneuvers naturally result.

consideration involves freeform mainfield lanes, and multiple tight edges for transitions to and from the mainfield lanes and along the headland path.

The solution of proposed method is presented in Fig. 7. Parameters used throughout are stated in Table 1.

Fig. 8 shows a zoom-in for an alternative solution approach to Problem 1. Here, a Bezier-curve (Pastva (1998)) of third order is fitted to the 5-point PWA path. This requires the solution of a least-squares problem to identify parameters before the evaluation of a Bernstein polynomial. While the interpolating fit is smooth this method does not take vehicle actuation limits into account (as proposed LPs (6) and (7) do). The path is therefore in general not feasible to drive.

Solve times and sizes of LPs for Problem 1 and 2 are in Tables 2 and 3, respectively. Sizes of the LPs are typically larger for Problem 1, with a larger average number of constraints  $\bar{n}_{\text{cstrs}}$  and a larger average number of variables  $\bar{n}_u$ . Solve times are very small, which is encouraging for the general approach. All experiments were run on a laptop running Ubuntu 22.04 equipped with an Intel Core i9 CPU @5.50GHz×32 and 32 GB of memory. For the solution of the LPs Scipy's (cf. Virtanen et al. (2020)) linprog()-solver in default settings was used.

Fig. 9 illustrates a zoom-in for sprayed coverage area avoiding any area coverage gaps.

In view of precision agriculture and autonomous robot applications an empirical finding of this work was that planning of transitions between headland path and mainfield lanes based only on Dubins-paths is not a viable option. Signification closed-loop tracking errors would be expected. As shown in Fig. 5(a) there are significant deviations between Dubins path and the path that is actually feasible considering actuation rate limits, especially when using the minimal vehicle turning radius,  $R_{\text{Dubins}} = 5\text{m}$ , for Dubins planning.

For three different turning radii,  $R_{\text{Dubins}} \in \{5\text{m}, 5.33\text{m}, 7\text{m}\}$ , used in the reference path generation step (Step 1 of the hierarchical two-step algorithm), Table 4 illustrates the effect on

lateral deviations between the Dubins-path used for reference path generation and the final smoothed path resulting from the LP-solution when accounting for vehicle actuation limits. The effect of using different  $R_{\text{Dubins}}$  is significant. See also Fig. 5 for visualisation.

More illustrative examples are provided in Fig. 11.

## 5. Discussion

A general comment about importance of input data quality is made. The quality of results for data-dependent techniques is a function of input data. For very *edgy* field contour input data, as is the case for all 5 fields in Fig. 7 and 11, a decision has to be made: (i) achieving full area coverage but exceeding contours when planning a nonholonomic path (see Fig. 8), or (ii) permitting area coverage gaps but achieving a path with sprayed area fully inside field contours. Both objectives cannot be achieved simultaneously. According to the formulations of Problem 1 and 2 avoiding area coverage gaps is the priority of this paper. Objective (ii) is likewise not trivial and subject of future work.

By counter-examples, below discussion is meant to provide further supporting arguments for proposed method.

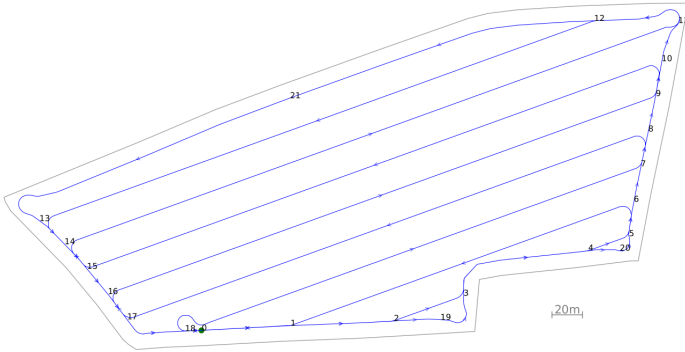
In Oh et al. (2023) a semi-analytic path planner using three consecutive clothoids is proposed. Using continuity conditions and boundary conditions for three clothoids 8 nonlinear algebraic equations with 15 variables are derived. Using algebraic manipulations these can be reduced to two nonlinear equations for the two unknowns, which can be solved using Newton's method and involving two tuning parameters. This method is interesting because of its analytic approach. However, it has three drawbacks that render it not suitable for our application. The first is that it is based on only three clothoids. This, however, is not sufficient to approximate all six combinations of Dubins paths (Dubins (1957)). To see this by counter-example, consider a RSR-combination (right turning, straight driving, right turning). The second disadvantage is that it is not straightforward how to adequately set the rate of curvature as a tuning parameter. For example, for Problem Type 1 steering is required that is not always fully operating at the actuating limits. To make a semi-analytic path planner work (after any extension of the approach to all 6 Dubins combinations), in such a scenario heuristics have to be devised and the method thereby evolves into a sampling scheme. The third limitation is that this analytic approach is limited to a specific vehicle model, namely one with no slip conditions at the front and the rear wheels and the center of gravity being located at the center of the rear axle.

In contrast, when extending the kinematic bicycle model (Rajamani (2011)) with slip to the model

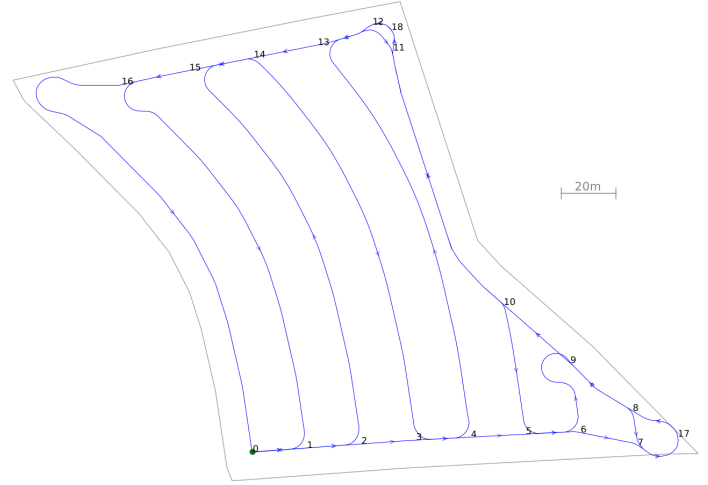
$$\begin{bmatrix} \dot{x} \\ \dot{y} \\ \dot{\psi} \\ \dot{v} \end{bmatrix} = \begin{bmatrix} v \cos(\psi + \beta) \\ v \sin(\psi + \beta) \\ \frac{v \cos(\beta)}{l} \tan(\delta) \\ a \end{bmatrix}, \quad (8)$$

where  $\beta = \arctan\left(\frac{g}{v}\right)$  denotes the slip angle,  $a$  denotes acceleration control, and the center of gravity is now located in the middle at distance  $\frac{l}{2}$  to both front and rear wheels, then the same conceptual approach described in this paper can be applied. The only difference is replacement of (1) with (8). See

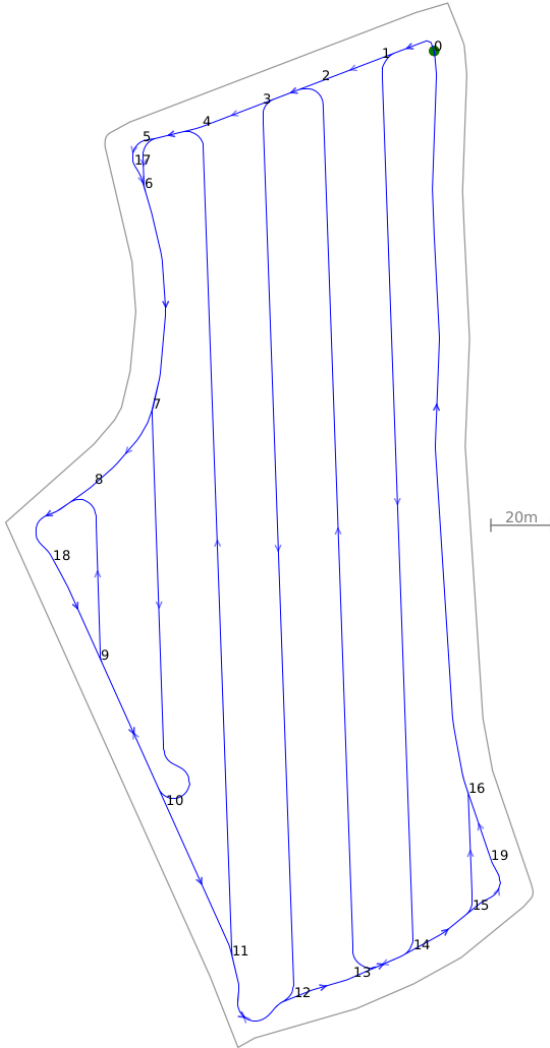
[0, 1, 2, 19, 3, 4, 20, 5, 6, 7, 8, 9, 10, 11, 12, 21, 13, 14, 15, 16, 17, 18, 0, 1, 2, 3, 4, 5, 6, 1, 0, 18, 7, 8, 17, 16, 9, 10, 15, 14, 11, 12, 13, 14, 15, 16, 17, 18, 0], operating width 20m



[0, 1, 2, 3, 4, 5, 6, 7, 17, 8, 9, 10, 11, 18, 12, 13, 14, 15, 16, 0, 1, 2, 15, 14, 3, 4, 13, 12, 11, 10, 5, 6, 9, 8, 7, 17, 8, 9, 10, 11, 18, 12, 13, 14, 15, 16, 1, 0], operating width 20m



[0, 1, 2, 3, 4, 5, 17, 6, 7, 8, 18, 9, 10, 11, 12, 13, 14, 15, 19, 16, 0, 1, 14, 13, 2, 3, 12, 11, 4, 5, 6, 7, 10, 9, 8, 18, 9, 10, 11, 12, 13, 14, 15, 16, 0], operating width 20m



[0, 1, 2, 3, 4, 5, 6, 37, 7, 8, 9, 10, 11, 12, 13, 14, 15, 16, 17, 18, 19, 20, 21, 22, 23, 24, 38, 25, 26, 27, 28, 29, 30, 31, 32, 33, 34, 35, 36, 0, 1, 2, 11, 10, 3, 4, 9, 8, 5, 6, 7, 8, 9, 10, 11, 12, 1, 0, 36, 13, 14, 35, 34, 15, 16, 33, 32, 17, 18, 31, 30, 19, 20, 29, 28, 21, 22, 27, 26, 23, 24, 25, 26, 27, 28, 29, 30, 31, 32, 33, 34, 35, 36, 0], operating width 20m

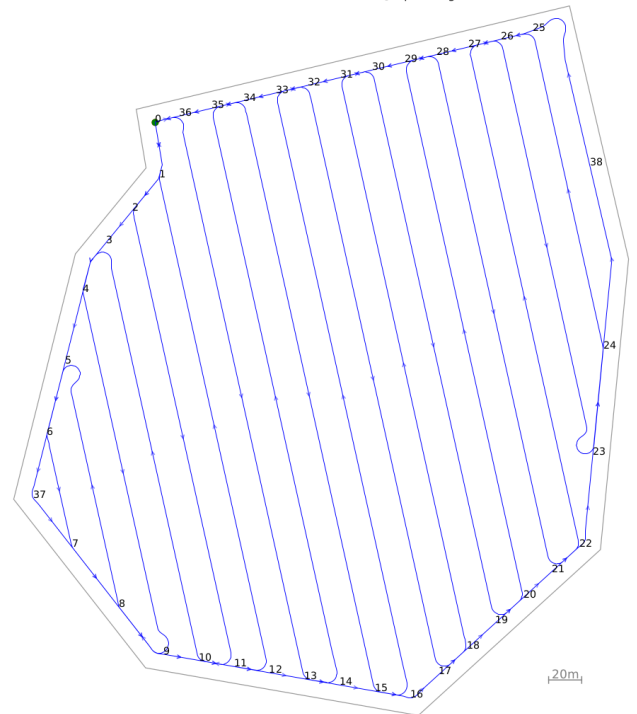


Fig. 11. More illustrative examples with edgy field contours: 3 fields with straight mainfield lanes and 1 field with freeform curved mainfield lanes. For each example, multiple instances of Problem 1 and Problem 2 had to be solved. Overall, 16 for Problem 1 and 68 for Problem 2.

also Miao et al. (2022) for an alternative vehicle model. Similarly, trailer dynamics can be incorporated (model equations are e.g. in Oksanen & Visala (2004), Plessen & Bemporad (2017)) into the proposed methodology.

Following similarly to Oh et al. (2023) an analytic approach and as earlier work within the agricultural context, Sabelhaus et al. (2013) is briefly discussed. They present analytic formulas and visualisations for 9 different symmetric lane-to-lane transitions (Omega-turn, U-turn, Gap-turn, Slope-turn,, Fishtail-turn,, Fishtail-turn with slope, Minimal longitudinal width, Pinhole-turn, Reversal pinhole turn) for continuous-curvature path planning. They also present three simulation experiments with longitudinal, lateral and angle offset of start and end point. Characteristically, all paths are constructed based on path segments with maximum curvature rate (clothoids with so called maximal sharpness) and circle segments with maximum curvature. Five comments are made. First, the methods are not suitable for Problem 1 since for that problem paths are needed that are not always and necessarily operating at the maximum curvature rate limit. Second and interestingly, in general none of the 9 cases can handle Problem 2 (e.g. for transitions as shown in Fig. 5). The Minimal longitudinal width-case resembles a transition as shown in Fig. 5, but it has a specific condition  $d = R_{\text{big}}$  (Sect. 2.3.7 in Sabelhaus et al. (2013)) that limits its usage. (Another reason herefore is that Sabelhaus et al. (2013) focus only on lane-to-lane transitions and not discuss headland-to-lane transitions.) Third, Sabelhaus et al. (2013) acknowledge that 'manoeuvres with start or end curvature  $\kappa \neq 0$  are not feasible with continuous curvature turns'. In contrast, for proposed LP-based method this case can be handled, by adding an initial input constraint  $\delta_0 = \delta_{\text{start}}$  or  $\delta_{N-1} = \delta_{\text{end}}$  to (6) or (7) for Problem 1 or 2, respectively, and by observing that curvature can be related to steering via  $\kappa = \frac{\tan(\delta)}{l}$  (for the assumption of no-slip conditions of the wheels and instantaneous curvature of the rear axle). This is made possible since the LP-based approach permits to incorporate state and input constraints in a structured manner. Fourth, as discussed for Oh et al. (2023), likewise the approach of Sabelhaus et al. (2013) is limited to a specific vehicle model (no slip condition). Fifth, the proposed spatial LP-method can also handle lane-to-lane transitions. For illustration see Fig. 10 with multiple non-symmetric start and end points and an interlane-distance of 5m. The simplicity of proposed method is underlined. For lane-to-lane transitions a Dubins-path is computed between the intersection points of headland path and mainfield lanes. The Dubins path is then used as reference path in the second hierarchical step solving a spatial-based LP to obtain a refined path. This paragraph underlines the flexibility of proposed method, in particular for shaping solutions to desired behavior.

A brief comment about path planning methods by neural networks is made (see a simplistic algorithm in Graf Plessen (2020) and the references therein). The key argument against the employment of neural networks is that both path planning Problems 1 and 2 deal with an *infinite* number of possible tasks for headland path edges and headland-to-mainfield

lane transitions and require a continuous action space. To encode a path planning module in a neural network an enormous number of training examples *and* their ground-truth solutions would be required, since there is an enormous variety in nature of different field contours, which would make a large training set mandatory. To underline the continuous control aspect, exemplarily see Plappert et al. (2018) where policies for continuous control are learned. However, each of the evaluation problems receives a reward either (i) upon *moving forward* (HalfCheetah, Hopper, Swimmer, Walker2D, SparseHalfCheetah, SwimmerGather), or (ii) upon reaching a *quasi-stationary* goal position (InvertedDoublePendulum, InvertedPendulum, Reacher, SparseCartpoleSwingup, SparseMountainCar, SparseDoublePendulum). There is no option for path shaping by accounting for precision constraints. Training time and hardware requirements are not stated. In contrast, proposed method is based on linear programming, with hyperparameter-free objective function, fast solve times, and can incorporate multivariate nonlinear vehicle dynamics and constraints on both states and control inputs in a structured manner to allow flexibility and generate deterministic precision paths, which is required for both Problems 1 and 2.

Peng et al. (2023) propose an optimisation-based algorithm in the time domain for headland turning under constraints imposed by headland geometry and obstacles, especially in orchard-like environments. In our paper obstacles in the headland are not assumed, however, since being a relevant problem the topic of obstacle avoidance within the spatial domain is briefly addressed. Based on previous work it is pointed to three options: (i) using a geometric path planner to solve the combinatorial corridor planning problem (Plessen et al. (2017a)), (ii) using a linearisation-approach to model obstacles in the spatial domain (Plessen et al. (2017b)), and (iii) using path corridor heuristics (Plessen (2017)). The last reference further discusses how velocity bounds within friction limits could be incorporated into spatial-based optimisation problems.

Finally, a comment about manual instead of autonomous driving is made. A visualisation such as Fig. 7 gives a farmer a reference path plan and practical guidance for how to steer. The importance of generated path plans for manual driving should not be underestimated, since the decision about how to drive transitions between headland path and mainfield lanes is often not straightforward in practice.

## 6. Conclusion

This paper contributed to the task of path planning within agricultural fields by proposing a method based on a spatial domain transformation of vehicle dynamics and linear programming to address the two tasks of smoothing of headland path edges and headland-to-mainfield lane transitions. Within the agricultural context this is the first paper suggesting to use a spatial domain vehicle dynamics representation in combination with a numerical optimisation approach to compute precision paths. Proposed method is of interest for both autonomous robot applications as well as as to provide high-level reference path plans for manual driving.

This paper is limited to forward-motion only. Methods can be extended to also permit backward-motion in the path planning, e.g., to permit three-point steering maneuvers involving both forward and backward motion at the transitions between headland path and mainfield lanes or headland path edges.

The main avenue of future work is the development of alternative heuristics to the 5-point piecewise-affine reference generation step for Problem Type 1.

## References

- Backman, J., Piirainen, P., & Oksanen, T. (2015). Smooth turning path generation for agricultural vehicles in headlands. *Biosystems Engineering*, *139*, 76–86.
- Boryga, M., Kołodziej, P., & Gołacki, K. (2020). Application of polynomial transition curves for trajectory planning on the headlands. *Agriculture*, *10*, 144.
- Bulgakov, V., Pascuzzi, S., Beloev, H., & Ivanovs, S. (2019). Theoretical investigations of the headland turning agility of a trailed asymmetric implement-and-tractor aggregate. *Agriculture*, *9*, 224.
- Chaikin, G. M. (1974). An algorithm for high-speed curve generation. *Computer graphics and image processing*, *3*, 346–349.
- Dubins, L. E. (1957). On curves of minimal length with a constraint on average curvature, and with prescribed initial and terminal positions and tangents. *American Journal of mathematics*, *79*, 497–516.
- Eski, İ., & Kuş, Z. A. (2019). Control of unmanned agricultural vehicles using neural network-based control system. *Neural Computing and Applications*, *31*, 583–595.
- Etezadi, H., & Eshkabilov, S. (2024). A comprehensive overview of control algorithms, sensors, actuators, and communication tools of autonomous all-terrain vehicles in agriculture. *Agriculture*, *14*, 163.
- Ettefagh, M. H., Naraghi, M., Towhidkhal, F., & Izi, H. (2018). Laguerre based model predictive control for trajectory tracking of nonholonomic mobile robots. In *RSI International Conference on Robotics and Mechatronics (IcRoM)* (pp. 298–303).
- Gao, G., Guo, H., Zhang, J., Zhang, Z., Wu, T., Lu, H., Qiu, Z., Chen, H., & Lingxuan, Z. (2023). An efficient headland-turning navigation system for a safflower picking robot. *Journal of Agricultural Engineering*, *54*.
- Graf Plessen, M. (2020). Automating vehicles by deep reinforcement learning using task separation with hill climbing. In *Advances in Information and Communication Conference (FICC), Volume 2* (pp. 188–210). Springer.
- Ha, J., Lee, C., Pal, A., Park, G., & Kim, H. (2018). Development of optimized headland turning mechanism on an agricultural robot for korean garlic farms. *Journal of Biosystems Engineering*, *43*, 273–284.
- He, Y., Zhou, J., Sun, J., Jia, H., Liang, Z., & Awuah, E. (2023). An adaptive control system for path tracking of crawler combine harvester based on paddy ground conditions identification. *Computers and Electronics in Agriculture*, *210*, 107948.
- Höffmann, M., Patel, S., & Büskens, C. (2024). Optimal guidance track generation for precision agriculture: A review of coverage path planning techniques. *Journal of Field Robotics*, *41*, 823–844.
- Jing, Y., Liu, G., & Luo, C. (2021). Path tracking control with slip compensation of a global navigation satellite system based tractor-scraper land leveling system. *Biosystems Engineering*, *212*, 360–377.
- Khan, A., Noreen, I., & Habib, Z. (2016). Coverage path planning of mobile robots using rational quadratic bézier spline. In *International Conference on Frontiers of Information Technology (FIT)* (pp. 319–323).
- Liu, J., Wu, X., Quan, L., Xu, H., & Hua, Y. (2024). Fuzzy adaptive pid control for path tracking of field intelligent weeding machine. *AIP Advances*, *14*.
- Miao, H., Diao, P., Xu, G., Yao, W., Song, Z., & Wang, W. (2022). Research on decoupling control for the longitudinal and lateral dynamics of a tractor considering steering delay. *Scientific Reports*, *12*, 13997.
- Mier, G., Valente, J., & de Bruin, S. (2023). Fields2cover: An open-source coverage path planning library for unmanned agricultural vehicles. *IEEE Robotics and Automation Letters*, *8*, 2166–2172.
- Oh, S., Chen, Q., Tseng, H. E., Pandey, G., & Orosz, G. (2023). Sharable clothoid-based continuous motion planning for connected automated vehicles. *arXiv preprint arXiv:2312.10880*, .
- Oksanen, T., & Visala, A. (2004). Optimal control of tractor-trailer system in headlands. In *Automation Technology for Off-Road Equipment Proceedings of the 2004 Conference* (p. 255). American Society of Agricultural and Biological Engineers.
- Pastva, T. A. (1998). *Bézier curve fitting*. Ph.D. thesis Monterey, California. Naval Postgraduate School.
- Peng, C., Wei, P., Fei, Z., Zhu, Y., & Vougioukas, S. G. (2023). Optimization-based motion planning for autonomous agricultural vehicles turning in constrained headlands. *Journal of Field Robotics*, .
- Pfeiffer, F., & Johanni, R. (1987). A concept for manipulator trajectory planning. *IEEE Journal on Robotics and Automation*, *3*, 115–123.
- Plappert, M., Houthoofd, R., Dhariwal, P., Sidor, S., Chen, R. Y., Chen, X., Asfour, T., Abbeel, P., & Andrychowicz, M. (2018). Parameter space noise for exploration. In *6th International Conference on Learning Representations (ICLR)*.
- Plessen, M. G. (2017). Trajectory planning of automated vehicles in tube-like road segments. In *IEEE International Conference on Intelligent Transportation Systems (ITSC)* (pp. 1–6).
- Plessen, M. G. (2019a). Coupling of crop assignment and vehicle routing for harvest planning in agriculture. *Artificial Intelligence in Agriculture*, *2*, 99–109.
- Plessen, M. G. (2019b). Optimal in-field routing for full and partial field coverage with arbitrary non-convex fields and multiple obstacle areas. *Biosystems Engineering*, *186*, 234–245.
- Plessen, M. G. (2021). Freeform path fitting for the minimisation of the number of transitions between headland path and interior lanes within agricultural fields. *Artificial Intelligence in Agriculture*, *5*, 233–239.
- Plessen, M. G., Bernardini, D., Esen, H., & Bemporad, A. (2017a). Spatial-based predictive control and geometric corridor planning for adaptive cruise control coupled with obstacle avoidance. *IEEE Transactions on Control Systems Technology*, *26*, 38–50.
- Plessen, M. G., Lima, P. F., Mårtensson, J., Bemporad, A., & Wahlberg, B. (2017b). Trajectory planning under vehicle dimension constraints using sequential linear programming. In *IEEE International Conference on Intelligent Transportation Systems (ITSC)* (pp. 1–6).
- Plessen, M. M. G. (2018). Partial field coverage based on two path planning patterns. *Biosystems Engineering*, *171*, 16–29.
- Plessen, M. M. G., & Bemporad, A. (2017). Reference trajectory planning under constraints and path tracking using linear time-varying model predictive control for agricultural machines. *Biosystems Engineering*, *153*, 28–41.
- Rajamani, R. (2011). *Vehicle dynamics and control*. Springer Science & Business Media.
- Sabelhaus, D., Röben, F., zu Helligen, L. P. M., & Lammers, P. S. (2013). Using continuous-curvature paths to generate feasible headland turn manoeuvres. *Biosystems engineering*, *116*, 399–409.
- Sun, Z., Wang, R., Meng, X., Yang, Y., Wei, Z., & Ye, Q. (2024). A novel path tracking system for autonomous vehicle based on model predictive control. *Journal of Mechanical Science and Technology*, *38*, 365–378.
- Trendafilov, K., & Tihanov, G. (2022). Comparative analysis of the idle move length when making t-turns by a mounted machine tractor unit in a field of irregular shape. *INMATEH-Agricultural Engineering*, *68*.
- Virtanen, P., Gommers, R., Oliphant, T. E., Haberland, M., Reddy, T., Cournapeau, D., Burovski, E., Peterson, P., Weckesser, W., Bright, J. et al. (2020). Scipy 1.0: fundamental algorithms for scientific computing in python. *Nature methods*, *17*, 261–272.
- Wang, H., & Noguchi, N. (2018). Adaptive turning control for an agricultural robot tractor. *International Journal of Agricultural and Biological Engineering*, *11*, 113–119.
- Wang, L., Chen, S., & Ren, H. (2024). An accurate trajectory tracking method for low-speed unmanned vehicles based on model predictive control. *Scientific reports*, *14*, 10739.
- Wang, Q., He, J., Lu, C., Wang, C., Lin, H., Yang, H., Li, H., & Wu, Z. (2023). Modelling and control methods in path tracking control for autonomous agricultural vehicles: A review of state of the art and challenges. *Applied Sciences*, *13*, 7155.
- Yin, C., Wang, S., Li, X., Yuan, G., & Jiang, C. (2020). Trajectory tracking based on adaptive sliding mode control for agricultural tractor. *IEEE Access*, *8*, 113021–113029.